



Research articles

Magneto-mechanical modeling of electrical steel sheets



U. Aydin^{a,*}, P. Rasilo^{a,b}, F. Martin^a, D. Singh^a, L. Daniel^c, A. Belahcen^a, M. Reikik^{c,d}, O. Hubert^d, R. Kouhia^e, A. Arkkio^a

^a Department of Electrical Engineering and Automation, Aalto University, Espoo, Finland

^b Laboratory of Electrical Energy Engineering, Tampere University of Technology, Tampere, Finland

^c Group of Electrical Engineering-Paris, CNRS (UMR 8507)/CentraleSuplec/UPMC/Université Paris-Sud, 3 rue Joliot-Curie, Plateau de Moulon, Gif-sur-Yvette, France

^d LMT (ENS Paris-Saclay/CNRS/Université Paris-Saclay), Cachan Cedex, France

^e Laboratory of Civil Engineering, Tampere University of Technology, Tampere, Finland

ARTICLE INFO

Article history:

Received 11 January 2017

Received in revised form 11 April 2017

Accepted 4 May 2017

Available online 5 May 2017

Keywords:

Magnetomechanical effects

Magnetostriction

Multiaxial stress

Multiscale modeling

ABSTRACT

A simplified multiscale approach and a Helmholtz free energy based approach for modeling the magneto-mechanical behavior of electrical steel sheets are compared. The models are identified from uniaxial magneto-mechanical measurements of two different electrical steel sheets which show different magneto-elastic behavior. Comparison with the available measurement data of the materials shows that both models successfully model the magneto-mechanical behavior of one of the studied materials, whereas for the second material only the Helmholtz free energy based approach is successful.

© 2017 Elsevier B.V. All rights reserved.

1. Introduction

Magnetostriction is a material property which causes deformation in the material when subject to magnetic field. Another phenomenon called Villari effect causes changes in the magnetic behavior of the material when mechanical stress is applied to it. Ferromagnetic materials exhibit both of these reciprocal features [1–8]. For some applications such as rotating electrical machines and transformers where ferromagnetic materials are widely used, these properties are usually adverse [9–16]. In most of these applications, the material is subject to multiaxial mechanical stresses which are caused by manufacturing processes or operating conditions [5,17–24]. In addition, the orientation of magnetic field and stress may vary in the material since, for instance, rotating electrical machines are subject to both rotating and alternating flux conditions. Earlier it was shown that the performance of rotating electrical machines is affected significantly by these complex multi-axial loadings [9–14]. In [15,16] it has been shown that magnetostriction clearly causes noise and vibrations in transformer cores. On the other hand, there are devices such as transducers, actuators, sensors and energy harvesters which are designed to benefit from magnetostriction and inverse magnetostriction properties of ferromagnetic materials [25–31]. Therefore, it is evident

that comprehensive magneto-mechanical characterization of ferromagnetic materials is needed in order to accurately analyze existing devices and design more efficient ones. Several studies have been done on modeling the multi-axial magneto-mechanical behavior of ferromagnetic materials [10,11,32–43]. For instance, in [11,33,34] the multi-axial modeling is performed with uniaxial models using an equivalent stress concept. Even though this modeling approach can be successful for some types of multiaxial configurations, it does not give a general description of the magneto-elastic behavior and can be inaccurate in some cases, particularly when the material is subject to bi-compression. A multiscale approach defining a local free energy at the domain scale and obtaining macroscopic magneto-elastic behavior by homogenization of local behavior is successful at modeling the multi-axial magneto-elastic behavior [35–38]. However, the implementation of multiscale models to numerical design tools is not favorable because of their computational cost. To reduce the computation time and keep benefit from the multiscale approach potentialities a simplified multiscale model has been developed for numerical computation tools. The computation speed is increased by around 1000 times compared to the full multiscale model [39,40]. The simplified multiscale approach requires only four physical based parameters to be identified, to the price of significant physical simplifications in the description of the magneto-elastic behavior. Another approach is taken in [41–43] by defining a Helmholtz free energy density which is a function of five scalar

* Corresponding author.

E-mail address: ugur.aydin@aalto.fi (U. Aydin).

invariants of the magneto-mechanical loading. The constitutive relations of the material are obtained by minimizing this energy. This modeling approach is also successful in predicting the multi-axial magneto-mechanical behavior of electrical steel sheets [43]. The number of required material parameters for the Helmholtz energy based model is material dependent. The objective of this paper is to compare a single-valued simplified multiscale (SM) model and a Helmholtz free energy based (HE) model which can both be used in numerical tools such as finite element analysis [39,41–43]. The SM approach [40] is used in its isotropic and anhysteretic version. The HE model is intrinsically isotropic and anhysteretic. Both models are identified from uniaxial magneto-mechanical measurements for two different materials which show different magneto-elastic behavior. In more detail, for Material I permeability increase under the whole studied tensile stress regime is observed. On the other hand, Material II shows increased permeability under low and decreased permeability under high tensile stress. Under compression the permeability deteriorates for both materials. Comparing the modelling results of the SM and HE models for these materials allows comprehensive analysis of the modeling abilities of these two approaches. After the identification process of the models, the anhysteretic magnetostriction modeling results under uniaxial loadings and magnetic modeling results under multi-axial magneto-mechanical loadings are compared with the available measurement data of the materials.

2. Magneto-mechanical models

2.1. Simplified multiscale (SM) model

The full version of the multiscale model [35–38] is based on a three-scale description of polycrystalline materials including the macroscopic (polycrystal), the single crystal (grain) and the magnetic domain scales. A localization procedure allows the definition of the local magneto-elastic loading at the grain scale from the knowledge of the macroscopic loading. A single crystal model is then defined from an energy description allowing to describe both domain motion and magnetization rotation. Appropriate homogenization procedures then allow retrieving the macroscopic response of the polycrystal. In the SM approach, in order to drastically reduce the computation time, the material is described as a fictitious single crystal with properties identified from the polycrystal behavior. This fictitious single crystal consists of a collection of randomly oriented magnetic domains. The free energy W_k of a domain is defined at the domain scale (k) as the sum of the magneto-static energy W_k^{mag} and the magneto-elastic energy W_k^{me} , and is given by

$$W_k = W_k^{\text{mag}} + W_k^{\text{me}} = -\mu_0 \mathbf{H} \cdot \mathbf{M}_k - \boldsymbol{\sigma} : \boldsymbol{\varepsilon}_k^{\text{II}} \quad (1)$$

where μ_0 is the permeability of free space, \mathbf{H} and $\boldsymbol{\sigma}$ are the applied magnetic field strength and mechanical stress, whereas \mathbf{M}_k and $\boldsymbol{\varepsilon}_k^{\text{II}}$ are the local magnetization and magnetostriction strain, respectively. An anisotropy energy term can be added to the free energy definition to describe the macroscopic anisotropy of the material [40]. In this work an isotropic material is assumed and this anisotropy energy term is not taken into account. For a domain oriented along \mathbf{u}_k the local magnetization \mathbf{M}_k and the local magnetostriction strain $\boldsymbol{\varepsilon}_k^{\text{II}}$ are classically given as

$$\mathbf{M}_k = M_s \mathbf{u}_k \quad (2)$$

$$\boldsymbol{\varepsilon}_k^{\text{II}} = \lambda_s \left(\frac{3}{2} \mathbf{u}_k \otimes \mathbf{u}_k - \frac{1}{2} \mathbf{I} \right) \quad (3)$$

where M_s and λ_s are the magnetization and macroscopic magnetostriction of the saturated material, respectively. \mathbf{I} is the second

order identity tensor. For a given set of domains with magnetization orientation \mathbf{u}_k the corresponding volume fraction f_k is introduced using a Boltzmann probability function [35]

$$f_k = \frac{\exp(-A_s W_k)}{\int_k \exp(-A_s W_k)} \quad (4)$$

where A_s is a model parameter that depends on the unstressed anhysteretic susceptibility χ_0 and is given by

$$A_s = \frac{3\chi_0}{\mu_0 M_s} \quad (5)$$

Using the defined volume fraction and an integration operation over all possible magnetization directions \mathbf{u}_k , the macroscopic magnetization \mathbf{M} and magnetostriction $\boldsymbol{\varepsilon}^{\text{II}}$ are obtained as the volume average of the corresponding local quantities:

$$\mathbf{M} = \langle \mathbf{M}_k \rangle = \int_k f_k \mathbf{M}_k \quad (6)$$

$$\boldsymbol{\varepsilon}^{\text{II}} = \langle \boldsymbol{\varepsilon}_k^{\text{II}} \rangle = \int_k f_k \boldsymbol{\varepsilon}_k^{\text{II}} \quad (7)$$

These integrations can be numerically performed by discretization of a unit sphere for the possible orientations \mathbf{u}_k [37].

In order to describe the non-monotonic effect of stress on magnetic permeability, a fictitious configuration field [38] is introduced as

$$\mathbf{H}_{\text{conf}} = \eta \left(N_\sigma - \frac{1}{3} \right) \mathbf{M} \quad (8)$$

where η is a dimensionless material parameter to be identified from uniaxial stress dependent magnetic measurements [38,40]. Function N_σ is

$$N_\sigma = \frac{1}{1 + 2 \exp(-K \sigma_{\text{eq}})} \quad (9)$$

$$K = \frac{3}{2} A_s \lambda_s \quad (10)$$

$$\sigma_{\text{eq}} = \frac{3}{2} \mathbf{h} \cdot \left(\boldsymbol{\sigma} - \frac{1}{3} \text{tr}(\boldsymbol{\sigma}) \mathbf{I} \right) \cdot \mathbf{h} \quad (11)$$

Here σ_{eq} is an equivalent stress defined as the projection of the deviatoric part of $\boldsymbol{\sigma}$ along the external applied magnetic field direction \mathbf{h} [33]. After calculating \mathbf{H}_{conf} the effective field \mathbf{H}_{eff} is obtained by adding up the external applied field \mathbf{H} and \mathbf{H}_{conf} as

$$\mathbf{H}_{\text{eff}} = \mathbf{H} + \mathbf{H}_{\text{conf}} \quad (12)$$

The four material parameters used in the SM model are M_s , λ_s , χ_0 and η . The corresponding identification procedure [40] is described in Section 3.

2.2. Helmholtz free energy based (HE) model

In this approach, the constitutive equations for coupling the magnetic and elastic properties of the material are derived from a Helmholtz free energy density ψ [41–43]. Considering an isotropic magneto-elastic material this energy density is a function of the magnetic flux density vector \mathbf{B} and the total strain tensor $\boldsymbol{\varepsilon}$, and can be expressed by the following six scalar invariants:

$$\begin{aligned} I_1 &= \text{tr}(\boldsymbol{\varepsilon}), \quad I_2 = \frac{1}{2} \text{tr}(\boldsymbol{\varepsilon}^2), \quad I_3 = \det(\boldsymbol{\varepsilon}) \\ I_4 &= \mathbf{B} \cdot \mathbf{B}, \quad I_5 = \mathbf{B} \cdot (\boldsymbol{\varepsilon} \mathbf{B}), \quad I_6 = \mathbf{B} \cdot (\boldsymbol{\varepsilon}^2 \mathbf{B}). \end{aligned} \quad (13)$$

Table 1
Parameter values for Material I and II (SM model).

Par.	Material I	Material II
M_s	$1.25 \cdot 10^6$ A/m	$1.26 \cdot 10^6$ A/m
λ_s	$7 \cdot 10^{-6}$	$7.35 \cdot 10^{-6}$
χ_0	$2.15 \cdot 10^3$	$11.57 \cdot 10^3$
η	0	$2.33 \cdot 10^{-4}$

Table 2
Parameter values for Material I and II (HE model).

Par.	Material I	Material II
α_0	$2.423 \cdot 10^{-4}$ J/m ³ T ²	$0.432 \cdot 10^{-4}$ J/m ³ T ²
α_1	$0.610 \cdot 10^{-4}$ J/m ³ T ⁴	$0.032 \cdot 10^{-4}$ J/m ³ T ⁴
α_2	$-1.487 \cdot 10^{-4}$ J/m ³ T ⁶	$1.267 \cdot 10^{-4}$ J/m ³ T ⁶
α_3	$6.435 \cdot 10^{-4}$ J/m ³ T ⁸	$-2.861 \cdot 10^{-4}$ J/m ³ T ⁸
α_4	$-9.935 \cdot 10^{-4}$ J/m ³ T ¹⁰	$3.358 \cdot 10^{-4}$ J/m ³ T ¹⁰
α_5	$7.408 \cdot 10^{-4}$ J/m ³ T ¹²	$-2.086 \cdot 10^{-4}$ J/m ³ T ¹²
α_6	$-2.617 \cdot 10^{-4}$ J/m ³ T ¹⁴	$0.661 \cdot 10^{-4}$ J/m ³ T ¹⁴
α_7	$0.365 \cdot 10^{-4}$ J/m ³ T ¹⁶	$-0.077 \cdot 10^{-4}$ J/m ³ T ¹⁶
β_0	$-5.398 \cdot 10^{-1}$ J/m ³ T ²	$-6.209 \cdot 10^{-1}$ J/m ³ T ²
β_1	-	833.9 J/m ³ T ⁴
β_2	-	$145.6 \cdot 10^4$ J/m ³ T ⁶
β_3	-	$-172.9 \cdot 10^7$ J/m ³ T ⁸
γ_0	372.498 J/m ³ T ²	$169.0 \cdot 10^1$ J/m ³ T ²
γ_1	-	$-983.4 \cdot 10^7$ J/m ³ T ⁴
γ_2	-	$168.8 \cdot 10^{14}$ J/m ³ T ⁶

The first three invariants describe purely mechanical loading. Since in this work linear elastic material is assumed ψ does not depend on I_3 . The fourth invariant I_4 is chosen to describe the single-valued magnetization behavior, whereas I_5 and I_6 describe the magneto-elastic coupling. In order to eliminate the effect of hydrostatic pressure on magnetic behavior in I_5 and I_6 , the deviatoric part of the strain $\tilde{\epsilon}$ is used. The Helmholtz free energy density $\psi(I_1, I_2, I_4, I_5, I_6)$ is then written as

$$\psi = \frac{1}{2} \lambda I_1^2 + 2GI_2 - v_0 \left(\frac{I_4}{2} + \sum_{i=0}^{n_x-1} \frac{\alpha_i}{i+1} I_4^{i+1} + \dots + \sum_{i=0}^{n_y-1} \frac{\beta_i}{i+1} I_5^{i+1} + \sum_{i=0}^{n_z-1} \frac{\gamma_i}{i+1} I_6^{i+1} \right). \quad (14)$$

Here λ and G are the Lamé constants of the material, v_0 is the reluctivity of free space and $\alpha_i, \beta_i, \gamma_i$ are the fitting parameters to be identified from measurements. The first two terms in (14) account for purely mechanical behavior, and the last two terms account for the magneto-mechanical coupling. The summation term in the middle accounts for the non-linear magnetic behavior under zero strain. The quadratic dependence of invariant I_6 on ϵ allows modeling the decreasing permeability under both compressive and high tensile stress.

The magnetization vector \mathbf{M} and the magneto-elastic stress tensor $\boldsymbol{\sigma}_{me}$ are expressed as the partial derivatives of ψ with respect to state variables \mathbf{B} and $\boldsymbol{\epsilon}$:

$$\mathbf{M}(\mathbf{B}, \boldsymbol{\epsilon}) = -\frac{\partial \psi(\mathbf{B}, \boldsymbol{\epsilon})}{\partial \mathbf{B}} \quad \text{and} \quad \boldsymbol{\sigma}_{me}(\mathbf{B}, \boldsymbol{\epsilon}) = \frac{\partial \psi(\mathbf{B}, \boldsymbol{\epsilon})}{\partial \boldsymbol{\epsilon}}. \quad (15)$$

The magnetic field strength vector is $\mathbf{H} = v_0 \mathbf{B} - \mathbf{M}$. The magneto-elastic stress tensor $\boldsymbol{\sigma}_{me}$ consists of elastic and magnetostriction related stress tensors.

3. Identification of the model parameters

Identification of the model parameters has been done for two different non-oriented (NO) Si-Fe electrical steel sheets from different suppliers. The grades of Material I and II are M330-50A and M400-50A, respectively.

The uniaxial experimental data from [5] is used to characterize the magneto-mechanical behavior of Material I. In the experiment process a cross-shaped sample which allows multiaxial magneto-mechanical loadings is used. The sample was loaded by stresses varying from 100 MPa compression (–) to 100 MPa tension (+) including biaxial ones. The surface magnetic field strength and the magnetic flux density were measured at 50 Hz using H -coils and needle probes, respectively. Only stress dependent magnetiza-

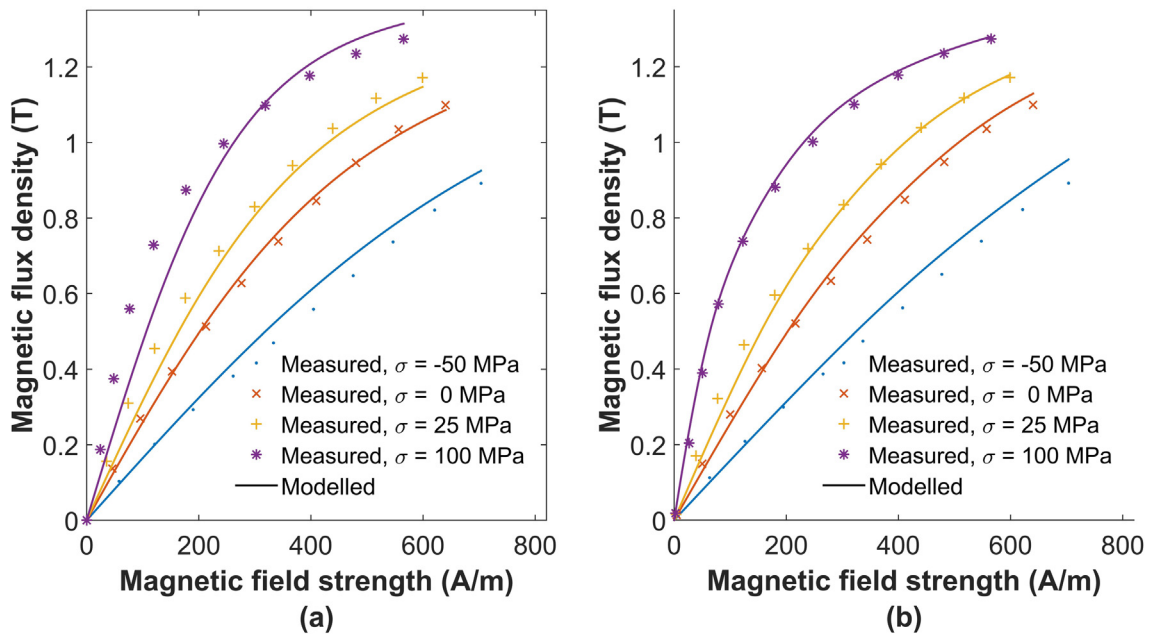


Fig. 1. Comparison of measured uniaxial stress dependent anhysteretic magnetization results with modeled results from (a) SM model and (b) HE model.

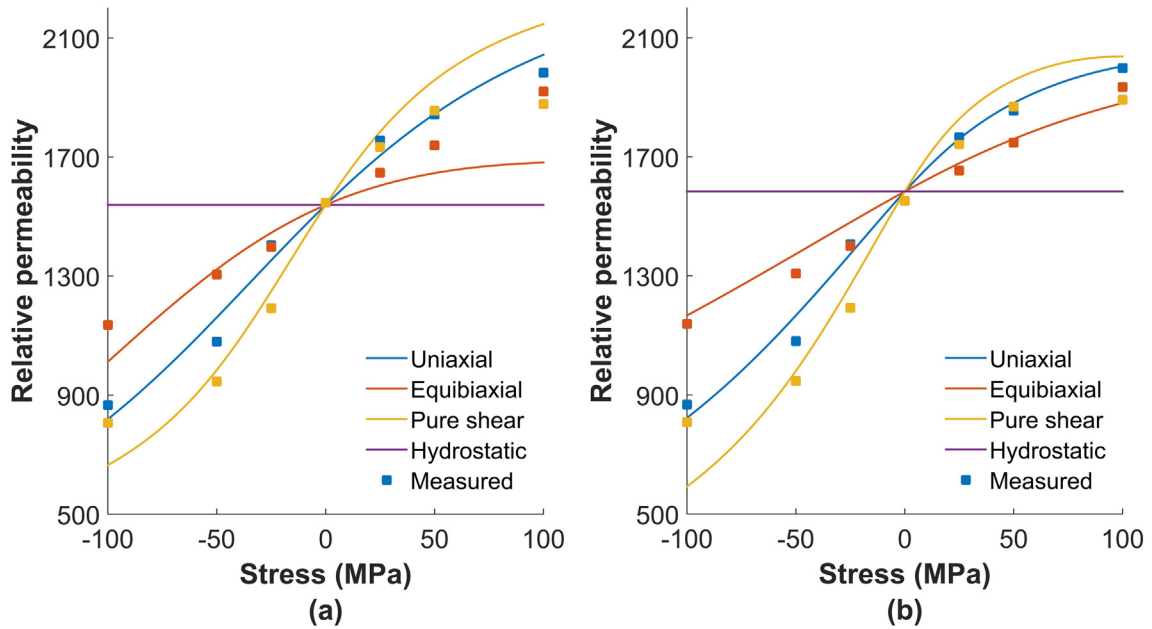


Fig. 2. Permeability evolution under multiaxial magneto-mechanical loadings for Material I. Measured permeabilities are shown with the markers. Results obtained from (a) the SM model and (b) the HE model.

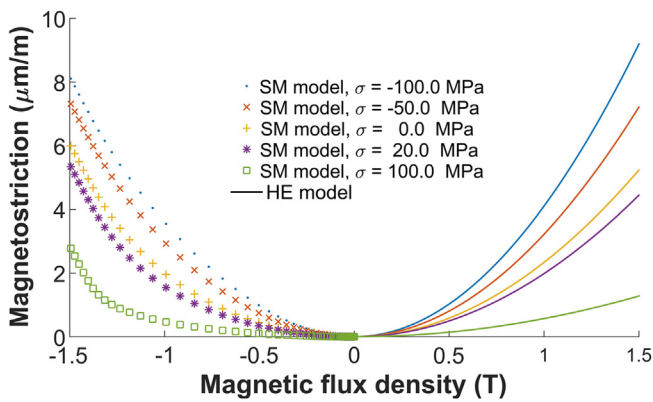


Fig. 3. Comparison of modeled uniaxial stress dependent magnetostriction for Material I.

tion curves were measured for Material I, not the magnetostriction. It is worth mentioning that in this experiment the measurement setup alone has non-negligible influence on the magnetic characteristics of the material. This influence causes approximately $\pm 10\%$ variation on the measured magnetic permeabilities of the specimen, which is placed into the setup, compared to the permeabilities of the free specimen [44].

On the other hand, the magneto-mechanical characteristics of Material II are obtained using experimental results from a custom built uniaxial single sheet tester [45]. In the experiment process a rectangular specimen was loaded with different stresses varying from -30 MPa to $+80$ MPa parallel to the flux density. A tunneling magneto-resistive sensor and a coil wound around the sample were used to measure the surface magnetic field strength and the magnetic flux density, respectively. Besides the magnetization curves, the magnetostriction was measured simultaneously using a rosette type strain gauge glued on the sample surface where the insulating coating was removed. The measurement frequency was 6 Hz.

The SM model requires four material parameters to model the anhysteretic magneto-mechanical behaviors of the Materials I and II. The parameters M_s , λ_s and χ_0 can be identified from macroscopic unstressed measurements. Since χ_0 represents the initial anhysteretic susceptibility it is identified from low-field measurements. Parameters M_s and λ_s can be taken as the maximum measured values for magnetization and magnetostriction measured parallel to the applied magnetic field [40]. In this work, M_s and χ_0 are identified for Materials I and II from the corresponding stress free magnetization measurements as in [40]. Therefore, it is expected to have smaller saturation magnetization M_s than its true value for 3% Si-Fe alloy [1]. Since for Material I the magnetostriction measurements are not available, λ_s is estimated from [36] for a 3% Si-Fe alloy. For Material II, λ_s is determined using single magnetostriction measurement under no applied stress.

The parameter η describes the non-monotonic magnetic behavior under stress and can be identified from the stress dependent magnetic measurements. The identification of η is realized for Materials I and II by least-squares fitting of the modeled uniaxial stress dependent magnetization curves to the measured ones under 100 MPa and 80 MPa, respectively. The determined parameter values for the SM model are given in Table 1 for both materials. It is worth noticing that the value of η for Material I is 0. This is because the magnetization behavior of Material I under tensile stress is monotonic. Therefore, configuration field H_{conf} is not needed. Whereas, the Material II shows non-monotonic behavior under tensile stress. In order to test the effectiveness of the configuration field H_{conf} for modelling this non-monotonic magneto-mechanical behavior of Material II the value of η is assumed to be 0 and $2.33 \cdot 10^{-4}$ where the latter one is identified from uniaxial magnetization measurement under 80 MPa.

On the other hand, in order to model the magneto-mechanical behaviors of Materials I and II, the HE model requires ten and fifteen material parameters, respectively. The reason for the need of higher number of model parameters for Material II is the non-monotonic magneto-mechanical behavior of this material under stress. In order to identify the model parameters for Material I the measured anhysteretic magnetization curves under uniaxial stresses of -50 MPa, 0 MPa, 25 MPa and 100 MPa, which are

applied parallel to magnetic field, are used. For Material II, the anhysteretic magnetization curves under uniaxial stress levels of -30 MPa, 0 MPa, 10 MPa and 80 MPa are used. For both materials, the parameters for HE model are identified by least squares fitting of the modeling results to the corresponding measured curves. The determined parameter values for the HE model for both materials are given in Table 2.

4. Results and discussion

4.1. Material I

The modeled magnetization curves by the SM and HE models are compared to measurements in Fig. 1(a) and (b), respectively. Both models predict the uniaxial magneto-mechanical behavior of Material I successfully. Under the studied uniaxial magneto-

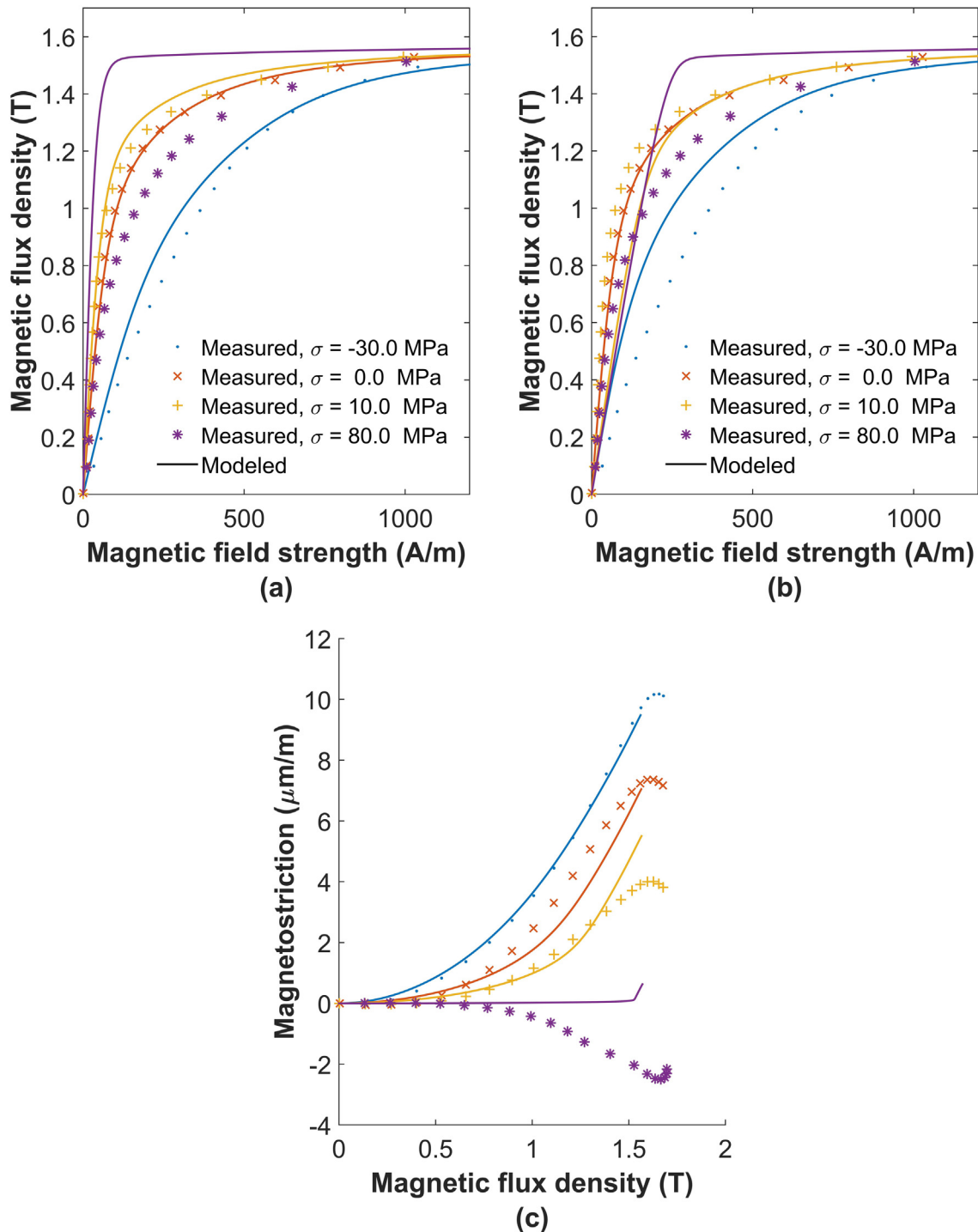


Fig. 4. Comparison of measured uniaxial stress dependent anhysteretic magnetization and magnetostriction with modeled results from SM model. (a) Anhysteretic magnetization results without H_{conf} ($\eta = 0$). (b) Anhysteretic magnetization with H_{conf} ($\eta = 2.33 \cdot 10^{-4}$). (c) Anhysteretic magnetostriction results. (Same legend as in Fig. 4(a) and (b).)

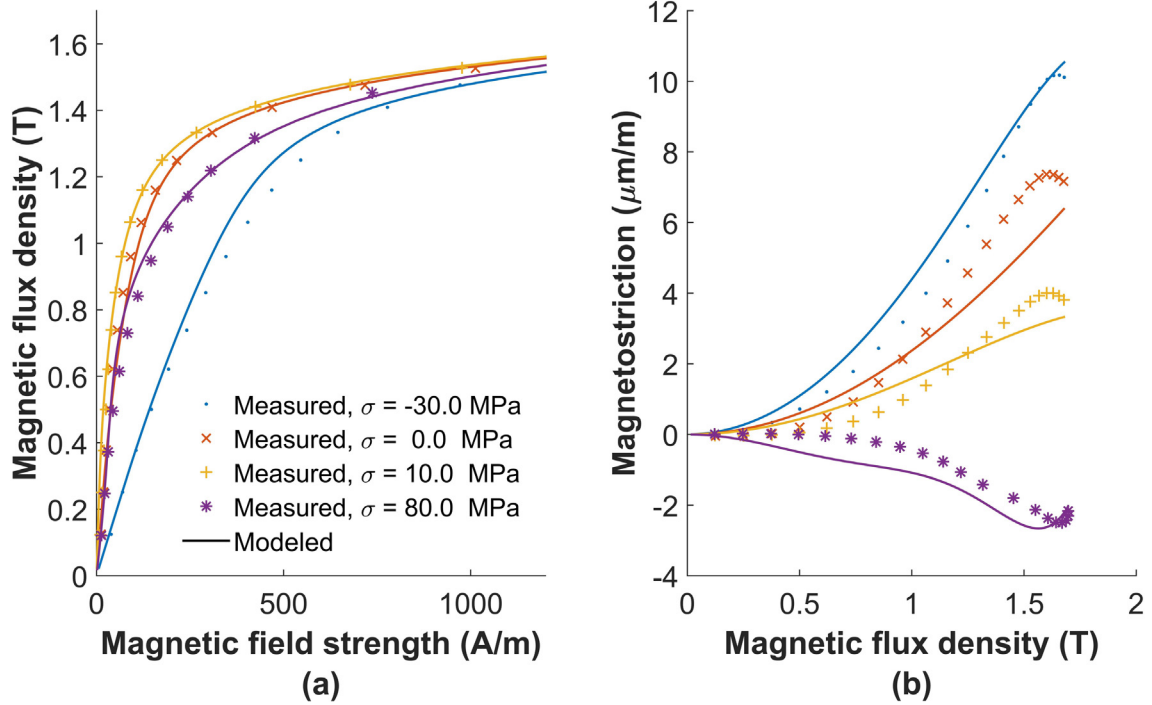


Fig. 5. Comparison of measured uniaxial stress dependent anhysteretic magnetization and magnetostriction with modeled results from HE model. (a) Anhysteretic magnetization and (b) anhysteretic magnetostriction results. (Same legend as in Fig. 5(a).)

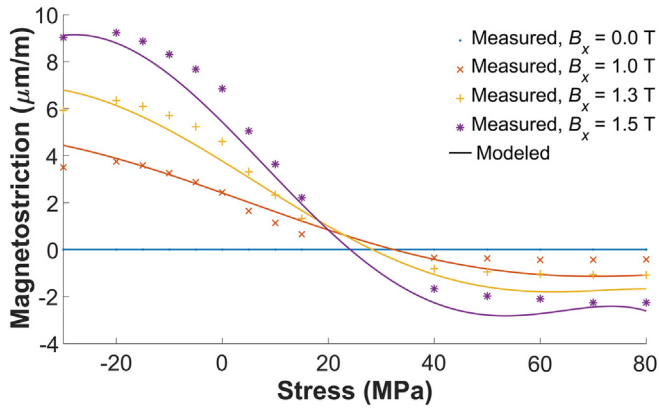


Fig. 6. Comparison between modeled and measured uniaxial stress depended magnetostriction under several induction levels applied along rolling direction (x) for Material II. Modeling results are obtained from the HE model.

mechanical loadings errors between the measured and modeled curves by SM model vary between 2% and 11%. Under the same loadings HE model produces slightly more accurate results with errors varying from 2% to 7%.

In order to analyze the magnetic behavior under multiaxial loadings, the following stress states are applied to the material:

$$\begin{aligned} \sigma_{\text{uni}} &= [\sigma \ 0 \ 0 \ 0 \ 0 \ 0]^T, & \sigma_{\text{equi}} &= [\sigma \ \sigma \ 0 \ 0 \ 0 \ 0]^T \\ \sigma_{\text{shear}} &= [\sigma \ -\sigma \ 0 \ 0 \ 0 \ 0]^T, & \sigma_{\text{hydro}} &= [\sigma \ \sigma \ \sigma \ 0 \ 0 \ 0]^T \end{aligned} \quad (16)$$

where σ_{uni} , σ_{equi} , σ_{shear} and σ_{hydro} represent uniaxial, equibiaxial, pure shear and hydrostatic stress states, respectively, and they are given in Voigt notation $\sigma = [\sigma_{xx} \ \sigma_{yy} \ \sigma_{zz} \ \sigma_{yz} \ \sigma_{zx} \ \sigma_{xy}]$. In (16) σ is the applied stress value. The material was simulated with ranging from -100 MPa to 100 MPa and under applied external

magnetic field of 500 A/m along the rolling direction. The applied magnetic field amplitude was chosen to be around the knee region of the magnetization curve under no applied stress. The modeled and measured permeability evolutions under these magneto-mechanical loadings are given in Fig. 2(a) and (b).

Considering the measurements, under uniaxial compression and tension the permeability decreases and increases, respectively, for every value of σ . When $\sigma < 0$ MPa, the pure shear stress affects the permeability more than the uniaxial and equibiaxial stress states. For 0 MPa $< \sigma \leq 50$ MPa the equibiaxial stress shows little effect on the permeability, whereas the pure shear stress causes similar effect as uniaxial stress. When -100 MPa $< \sigma < -50$ MPa and 100 MPa $> \sigma > 50$ MPa, the effect of uniaxial and pure shear stresses on permeability starts to decrease. Similar decreased rate of change on permeability has also been observed in [46,47] for NO electrical steel under high uniaxial stress levels. The modeling results from SM and HE approaches are close to each other. They show reasonable agreement with the measurements between -50 MPa and 50 MPa for all the stress states. At higher stress values both models overestimate the effect of pure shear stress on the permeability. Besides, the SM model underestimates the permeability considerably under the equibiaxial stress state above 50 MPa. It is also worth noticing that both models produce constant permeability under hydrostatic pressure which is consistent with the magneto-elastic theories. The modeled magnetostriction curves obtained from both models under several uniaxial stresses and up to 1.5 T flux density are given in Fig. 3. The resulting magnetostriction behaviors are consistent with each other.

4.2. Material II

As mentioned earlier, magneto-mechanical measurements show that Material II exhibits different magneto-mechanical behavior compared to Material I. Particularly, the permeability of Material II has non-monotonic dependency on uniaxial stress, so that both compression and high tensile stress reduce the perme-

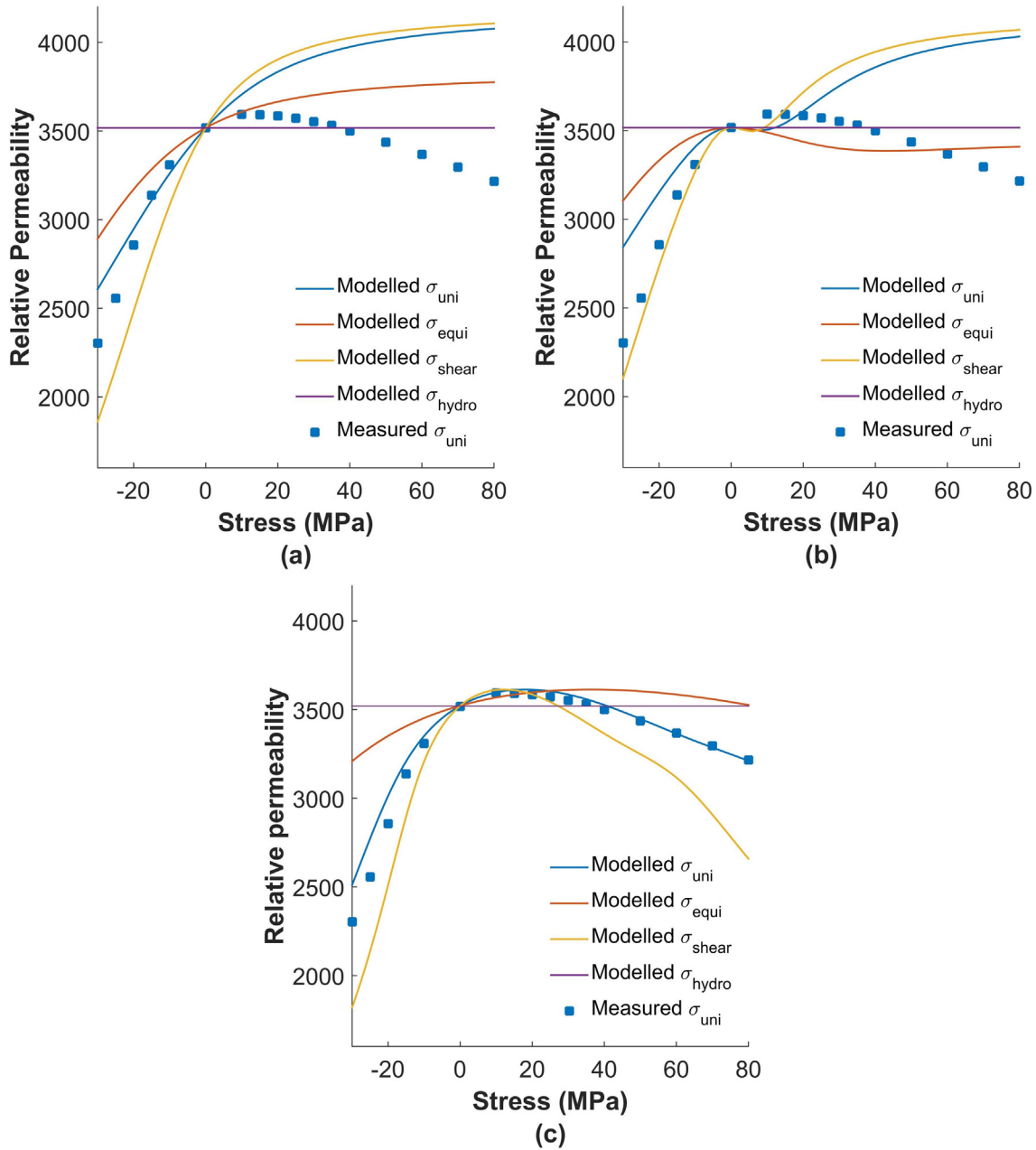


Fig. 7. Permeability evolution under multiaxial magneto-mechanical loadings for Material II. Measured uniaxial permeabilities are shown with the markers. (a) SM model results without \mathbf{H}_{conf} ($\eta = 0$), (b) SM model results with \mathbf{H}_{conf} ($\eta = 2.33 \cdot 10^{-4}$), (c) HE model results.

ability. Also magnetostriction reversal is observed from positive to negative when sufficient tensile stress is applied.

Despite the configuration field term \mathbf{H}_{conf} which was introduced to take into account the non-monotonic magnetization behavior under stress, modeling the magneto-mechanical behavior of the Material II by using SM model was unsuccessful. In order to demonstrate this, results from SM model without and with \mathbf{H}_{conf} under four different uniaxial stress levels compared to measurements in Fig. 4(a) and (b). When there is no \mathbf{H}_{conf} ($\eta = 0$), the model is reasonably accurate for compression and low tensile stress regimes, whereas, it is not successful under high tensile stress. Introducing \mathbf{H}_{conf} with determined parameter $\eta = 2.33 \cdot 10^{-4}$, results in slightly more accurate description of magnetization behavior under high tensile stress. However, results under compression and low tensile become inaccurate compared to the case when there is no \mathbf{H}_{conf} . This results indicate that the use of \mathbf{H}_{conf}

with SM model is not sufficient to take into account the non-monotonic magneto-mechanical behavior of Material II. On the other hand, the magnetostriction modeling results by SM model are independent of \mathbf{H}_{conf} . In Fig. 4(c) modeled anhysteretic magnetostriction curves by the SM model are compared to the measured ones under several uniaxial stresses. Although, under compression and low tensile results are reasonably accurate, under high tensile stress considerable difference is observed compared to measurements.

Modeling such non-monotonic magneto-mechanical behavior as observed for Material II with the simplified multiscale approach is still under study. A possibility to improve the description of such a behavior by SM model would be to introduce a uniaxial stress dependent macroscopic saturation magnetostriction parameter instead of constant λ_s . To do that, one would need stress dependent magneto-mechanical measurements. Another approach can be

modifying the configuration field given in (8) and defining a configuration magnetostriction using the stress dependent magnetostriction data with the expense of introducing more material parameters. The improvement of the SM model is out of the scope of this paper, and will be part of further studies. Fig. 5(a) and (b) show the modeling results for the anhysteretic magnetization and magnetostriction curves obtained using the HE model under four uniaxial stress levels. The model is able to take into account the non-monotonic dependency of the permeability on the stress. In addition, flipping of the magnetostriction curve with respect to the axis of abscissa at high tensile stress is successfully modeled. In order to analyze the magnetostriction behavior of the HE model more closely, the magnetostriction is calculated under different uniaxial stress levels and comparison to the measurements at several induction magnitudes are given in Fig. 6. The results are in reasonable agreement with the measurements when the material is subject to both compressive and tensile stresses. However, despite the fact that the modeled magnetostriction curves are close to the measured ones, the magnetostriction rotation under high magnetic flux density is not well taken into account.

The permeability evolutions are modeled using both models for Material II under the stress states given in (16) with σ ranging from -30 MPa to 80 MPa and under applied external magnetic field of 300 A/m along the rolling direction. The applied magnetic field amplitude was chosen to be around the knee region of the measured magnetization curve under no applied stress. The results obtained from SM model without and with H_{conf} are given in Fig. 7(a) and (b), respectively. In addition, the measured permeabilities under uniaxial loadings are shown with markers. Hydrostatic pressure does not affect the permeability which is modeled consistently by both cases. When there is no H_{conf} , the results are in reasonable agreement with the measurements under uniaxial compression. However, under uniaxial tensile stress, model shows very different behavior compared to the measurements. Including H_{conf} does not improve the accuracy for both compression and tensile stress regime. Therefore, it is expected that the SM model will be inaccurate also for the equibiaxial and pure shear stress cases under tensile stress regime. Under compressive stress regime, pure shear stress reduce the permeability considerably more than equibiaxial stress.

The permeability evolution results from HE model are given in Fig. 7(c) under aforementioned magneto-mechanical loadings. Under uniaxial stress the modeling results are in agreement with the measurements for the studied stress levels. Considering the studied multiaxial stress states, hydrostatic pressure does not have any effect on the permeability which is consistent with the theory. Equibiaxial stress causes slight variation, whereas, the pure shear stress causes the largest effect on the permeability.

5. Conclusion

Two different magneto-mechanical models were compared. The first model (SM) is a simplified version of a multiscale approach and it defines the magneto-elastic behavior of the material based on the free energy in the domain scale. On the other hand, the second model (HE) describes the magneto-elastic behavior by obtaining constitutive equations from a Helmholtz free energy density expressed as a function of five scalar invariants. The SM model requires only four physical based parameters to provide predictions for magneto-elastic behavior. The number of parameters to model the magneto-mechanical behavior by the HE model is material dependent and a set of uniaxial magneto-mechanical measurements are required for the identification of these parameters. The two models were applied to two different materials which show different

magneto-mechanical characteristics. Particularly, the permeability of Material I increases under the whole studied tensile stress regime, whereas Material II shows increased permeability under low and decreased permeability under high tensile stress. Under compression the permeability decreases for both materials. The comparisons with the measurements under uniaxial and biaxial stresses show that both models predict the magnetic behavior of Material I with reasonable accuracy up to ± 50 MPa stress levels. Also, both models produce similar uniaxial stress dependent magnetostriction behavior for this material. The SM model reveals its limitations during the comparisons of modeling results to the magneto-mechanical measurements of Material II. In order to model the magneto-mechanical behavior as observed for Material II, the SM model would require modifications. On the other hand, comparisons to the measurements show that the presented HE model can model the uniaxial magneto-mechanical behavior of Material II consistently. A limitation of the HE model is its poor prediction ability outside the range of identified stress levels. Therefore, it is recommended to use the HE model up to the highest stress level for which it is identified. On the other hand, once identified, the presented SM model can predict the magneto-mechanical behavior of the materials, whose permeability shows monotonic dependency on stress, up to high stress levels within the elastic limits. Comparison of the magneto-mechanical modeling abilities of the two models exhibits their differences and complementarities. When very limited experimental measurements are available on the material, the SM approach provides a very simple identification procedure and reasonable predictions. When a more comprehensive characterization of the material is available, the HE model relies on detailed fitting procedures that allow a more accurate description of the material behavior. It can also be mentioned that the full multiscale approaches, incorporating a more complete description of the physical mechanisms at play could also be a promising option to identify the HE model parameters when insufficient experimental data is available.

Acknowledgments

The research leading to these results has received funding from the European Research Council under the European Union's Seventh Framework Programme (FP7/2007-2013)/ ERC grant agreement n° 339380. P. Rasilo and F. Martin acknowledge the Academy of Finland for financial support under grants 274593 and 13297345.

References

- [1] R.M. Bozorth, *Ferromagnetism*, Van Nostrand Company, New York, 1951, pp. 67–101, 595–712.
- [2] Y. Kai, Y. Tsuchida, T. Todaka, M. Enokizono, Influence of biaxial stress on vector magnetic properties and 2-D magnetostriction of a nonoriented electrical steel sheet under alternating magnetic flux conditions, *IEEE Trans. Magn.* 50 (4) (Apr. 2014) 6100204.
- [3] Y. Kai, Y. Tsuchida, T. Todaka, M. Enokizono, Influence of stress on vector magnetic property under alternating flux conditions, *IEEE Trans. Magn.* 47 (Oct. 2011) 4344–4347.
- [4] P.I. Anderson, A.J. Moses, H.J. Stanbury, Assessment of the stress sensitivity of magnetostriction in grain-oriented silicon steel, *IEEE Trans. Magn.* 43 (8) (Aug. 2007) 3467–3476.
- [5] M. Rekić, O. Hubert, L. Daniel, Influence of a multiaxial stress on the reversible and irreversible magnetic behaviour of 3% Si-Fe alloy, *Int. J. Appl. Electromagn. Mech.* 44 (3–4) (Mar. 2014) 301–315.
- [6] O. Perevertov, J. Thielsch, R. Schäfer, Effect of applied tensile stress on the hysteresis curve and magnetic domain structure of grain-oriented transverse Fe-3%Si steel, *J. Magn. Magn. Mater.* 385 (Jul. 2015) 358–367.
- [7] O. Perevertov, Influence of the applied elastic tensile and compressive stress on the hysteresis curves of Fe-3%Si non-oriented steel, *J. Magn. Magn. Mater.* 428 (Apr. 2017) 223–228.

- [8] S. Bao, Y. Gu, M. Fu, D. Zhang, S. Hu, Effect of loading speed on the stress-induced magnetic behavior of ferromagnetic steel, *J. Magn. Magn. Mater.* 423 (Feb. 2017) 191–196.
- [9] K. Delaere, W. Heylen, R. Belmans, K. Hameyer, Comparison of induction machines stator vibration spectra induced by reluctance forces and magnetostriction, *IEEE Trans. Magn.* 38 (2) (Mar. 2002) 969–972.
- [10] S. Zeze, Y. Kai, T. Todaka, M. Enokizono, Vector magnetic characteristic analysis of a pm motor considering residual stress distribution with complex-approximated material modelling, *IEEE Trans. Magn.* 48 (11) (Nov. 2012) 3352–3355.
- [11] K. Yamazaki, Y. Kato, Iron loss analysis of interior permanent magnet synchronous motors by considering mechanical stress and deformation of stators and rotors, *IEEE Trans. Magn.* 50 (2) (Feb. 2014) 7022504.
- [12] Y. Kai, Y. Tsuchida, T. Todaka, M. Enokizono, Effect of local residual stress in rotating machine core on vector magnetic property, in *Proc. Int. Conf. Electr. Mach., ICEM, Rome, Italy, Sep. 6–8 2010*, pp. 1–6.
- [13] D. Miyagi, N. Maeda, Y. Ozeki, K. Miki, N. Takashi, Estimation of iron loss in motor core with shrink fitting using fem analysis, *IEEE Trans. Magn.* 45 (3) (Mar. 2009) 1704–1707.
- [14] A.A. Abdallah, L. Dupré, The influence of magnetic material degradation on the optimal design parameters of electromagnetic devices, *IEEE Trans. Magn.* 50 (4) (Apr. 2014) 1–10.
- [15] B. Weiser, H. Pfützner, J. Anger, Relevance of magnetostriction and forces for the generation of audible noise of transformer cores, *IEEE Trans. Magn.* 36 (Sep. 2000) 3759–3777.
- [16] R. Penin, J.P. Lecointe, G. Parent, J.F. Brudny, T. Belgrand, Grain-oriented steel rings for an experimental comparison of relative magnetostriction and Maxwell's forces effects, *IEEE Trans. Ind. Electron.* 61 (8) (Aug. 2014) 4374–4382.
- [17] S.K. Kuo, W.C. Lee, S.Y. Lin, C.Y. Lu, The influence of cutting edge deformations on magnetic performance degradation of electrical steel, *IEEE Trans. Ind. Appl.* 51 (6) (2015) 4357–4363.
- [18] A. Pulnikov, P. Baudouin, J. Melkebeek, Induced stresses due to the mechanical cutting of non-oriented electrical steels, *J. Magn. Magn. Mater.* 254–255 (Jan. 2003) 355–357.
- [19] D. Gerada, A. Mebarki, N.L. Brown, K.J. Bradley, C. Gerada, Design aspects of high-speed high-power-density laminated-rotor induction machines, *IEEE Trans. Ind. Electron.* 58 (9) (Sep. 2011) 4039–4047.
- [20] A. Borisavljevic, H. Polinder, J.A. Ferreira, On the speed limits of permanent-magnet machines, *IEEE Trans. Ind. Electron.* 57 (1) (Jan. 2010) 220–227.
- [21] F. Chai, Y. Li, P. Liang, Y. Pei, Calculation of the maximum mechanical stress on the rotor of interior permanent magnet synchronous motors, *IEEE Trans. Ind. Electron.* 63 (6) (2016) 3420–3432.
- [22] D.J.B. Smith, B.C. Mcrow, G.J. Atkinson, A.G. Jack, A.A.A. Mehna, Shear stress concentrations in permanent magnet rotor sleeves, in: *Proc. Int. Conf. Electr. Mach., ICEM, Rome, Italy, Sep. 6–8 2010*, pp. 1–6.
- [23] P. Baudouin, A. Belhadj, F. Breaban, A. Deffontaine, Y. Houbaert, Effects of laser and mechanical cutting modes on the magnetic properties of low and medium Si content nonoriented electrical steels, *IEEE Trans. Magn.* 38 (5) (Sep. 2002) 3213–3215.
- [24] Y. Kai, Y. Tsuchida, T. Todaka, M. Enokizono, Evaluation of local residual stress distribution of stator core in rotating machine, *IEEJ Trans. FM* 131 (5) (May 2011) 389–394.
- [25] A.G. Olabi, A. Grunwald, Design and application of magnetostrictive materials, *Mater. Des.* 29 (2) (2008) 469–483.
- [26] P. Li, Y. Wen, W. Yin, H. Wu, An upconversion management circuit for low-frequency vibrating energy harvesting, *IEEE Trans. Ind. Electron.* 61 (7) (Jul. 2014) 3349–3358.
- [27] P. Li, Y. Wen, C. Jia, X. Li, A magnetolectric composite energy harvester and power management circuit, *IEEE Trans. Ind. Electron.* 58 (7) (Jul. 2011) 2944–2951.
- [28] X. Zhao, D.G. Lord, Application of the Villari effect to electric power harvesting, *J. Appl. Phys.* 99 (8) (Apr. 2006) 08M703.
- [29] H.B. Wang, A highly sensitive magnetometer based on the Villari effect, *IEEE Trans. Magn.* 49 (4) (Apr. 2013) 1327–1333.
- [30] D.E. Mouzakis, D. Dimogianopoulos, D. Giannikas, Contact-free magnetoelastic smart microsensors with stochastic noise filtering for diagnosing orthopedic implant failures, *IEEE Trans. Ind. Electron.* 56 (4) (Apr. 2009) 1092–1100.
- [31] R.V. Petrov, V.M. Petrov, M.I. Bichurin, Y. Zhou, S. Priya, Modeling of dimensionally graded magnetolectric energy harvester, *J. Magn. Magn. Mater.* 383 (Jun. 2015) 246–249.
- [32] J. Pearson, P.T. Squire, M.G. Maylin, J.G. Gore, Biaxial stress effects on the magnetic properties of pure iron, *IEEE Trans. Magn.* 36 (5) (Sep. 2000) 3251–3523.
- [33] L. Daniel, O. Hubert, An equivalent stress for the influence of multiaxial stress on the magnetic behavior, *J. Appl. Phys.* 105 (2009) 07A313.
- [34] O. Hubert, L. Daniel, Energetical and multiscale approaches for the definition of an equivalent stress for magneto-elastic couplings, *J. Magn. Magn. Mater.* 323 (13) (2011) 1766–1781.
- [35] N. Buiron, L. Hirsinger, R. Billardon, A multiscale model for magneto-elastic couplings, *J. Phys. IV France*, vol. 9, no. PR9, pp. PR9-187-PR9-196, Sep. 1999.
- [36] L. Daniel, O. Hubert, R. Billardon, Homogenisation of magneto-elastic behaviour: from grain to the macro scale, *Comp. Appl. Math.* 23 (2–3) (2004) 285–308.
- [37] L. Daniel, N. Galopin, A constitutive law for magnetostrictive materials and its application to terfenol-d single and polycrystals, *Eur. Phys. J. Appl. Phys.* 42 (2) (May 2008) 153–159.
- [38] L. Daniel, M. Rekik, O. Hubert, A multiscale model for magneto-elastic behaviour including hysteresis effects, *Arch. Appl. Mech.* 84 (9) (May 2014) 1307–1323.
- [39] L. Bernard, X. Mininger, L. Daniel, G. Krebs, F. Bouillault, M. Gabsi, Effect of stress on switched reluctance motors: a magneto-elastic finite-element approach based on multiscale constitutive laws, *IEEE Trans. Magn.* 47 (9) (Sep. 2011) 2171–2178.
- [40] L. Daniel, O. Hubert, M. Rekik, A simplified 3-D constitutive law for magnetomechanical behavior, *IEEE Trans. Magn.* 51 (3) (Mar. 2015).
- [41] K.A. Fonteyn, A. Belahcen, R. Kouhia, P. Rasilo, A. Arkkio, FEM for directly coupled magneto-mechanical phenomena in electrical machines, *IEEE Trans. Magn.* 46 (8) (Aug. 2010) 2923–2926.
- [42] K.A. Fonteyn, Energy-based magneto-mechanical model for electrical steel sheets (Ph.D. thesis), Aalto University, Espoo, Finland, 2010.
- [43] U. Aydin, P. Rasilo, D. Singh, A. Lehtikoinen, A. Belahcen, A. Arkkio, Coupled magneto-mechanical analysis of iron sheets under biaxial stress, *IEEE Trans. Magn.* 52 (3) (Mar. 2016) 2000804.
- [44] O. Hubert, Influence of biaxial stresses on the magnetic behavior of iron-cobalt sheet – experiments and modelling, *Przeglad Elektrotechniczny* 83 (4) (2007) 70–77.
- [45] D. Singh, P. Rasilo, F. Martin, A. Belahcen, A. Arkkio, Effect of mechanical stress on excess loss of electrical steel sheets, *IEEE Trans. Magn.* 51 (11) (Nov. 2015) 1001204.
- [46] D. Miyagi, K. Miki, M. Nakano, N. Takahashi, Influence of compressive stress on magnetic properties of laminated electrical steel sheets, *IEEE Trans. Magn.* 46 (2) (Feb. 2010) 318–321.
- [47] V.E. Iordache, E. Hug, N. Buiron, Magnetic behavior versus tensile deformation mechanisms in a non-oriented Fe-(3 wt.%Si) steel, *J. Magn. Magn. Mater.* 359 (1–2) (2003) 62–74.